J. Fluid Mech. (2003), *vol.* 480, *pp.* 65–94.
DOI: 10.1017/S0022112002003567 Printed in the United Kingdom

Stability of symmetric vortices in two dimensions and over three-dimensional slender conical bodies

By JINSHENG CAI[1], FENG LIU[1] AND SHIJUN LUO[2]

[1]Department of Mechanical and Aerospace Engineering, University of California, Irvine, CA 92697-3975, USA

[2]Department of Aircraft Engineering, Northwestern Polytechnical University, Xi'an, China

(Received 20 December 2001 and in revised form 25 October 2002)

A general stability condition for vortices in a two-dimensional incompressible inviscid flow field is presented. This condition is first applied to analyse the stability of symmetric vortices behind elliptic cylinders and circular cylinders with a splitter plate at the rear stagnation point. The effect of the size of the splitter plate on the stability of the vortices is studied. It is also shown that no stable symmetric vortices exist behind two-dimensional bodies based on the stability condition. The two-dimensional stability condition is then extended to analyse the absolute (temporal) stability of a symmetric vortex pair over three-dimensional slender conical bodies. The three-dimensional problem is reduced to a vortex stability problem for a pair of vortices in two dimensions by using the conical flow assumption, classical slender-body theory, and postulated separation positions. The bodies considered include circular cones and highly swept flat-plate wings with and without vertical fins, and elliptic cones of various eccentricities. There exists an intermediate cone with a finite thickness ratio between the circular cone and the flat-plate delta wing for which the symmetric vortices change from being unstable to being stable at a given angle of attack. The effects of the fin height and the separation position on the stability of the vortices are studied. Results agree well with known experimental observations.

1. Introduction

Separation vortices over highly swept wings and slender bodies at high angles of attack are known to greatly increase the lift coefficient. However, the initially symmetric vortices may become asymmetric as the angle of attack is increased beyond a certain value, causing large rolling moments in the case of swept wings or large side forces in the case of slender bodies even at zero roll and yawing angles. The transition of the vortex pattern from being symmetric to asymmetric is of major importance for the performance and control of aircraft and other flight vehicles capable of extreme manoeuvres. Much experimental, theoretical and computational work has been performed on the understanding, prediction, and control of the onset of vortex asymmetry (for example, Thomson & Morrison 1971; Keener & Chapman 1977; Zilliac, Degani & Tobak 1991; Pidd & Smith 1991; Degani 1992; Degani & Levy 1992; Degani & Tobak 1992; Ericsson & Reding 1992; Levy, Hesselink, & Degani 1996; Bernhardt & Williams 1998; and references cited therein). The basic physical mechanism of this transition, however, is not clear. At least two possible causes for the vortex asymmetry have been suggested mainly based on

experimental investigations: (i) inviscid hydrodynamic instability of the symmetrically separated vortices (Keener & Chapman 1977); (ii) asymmetric flow separation and/or asymmetric flow reattachment on each side of the body (Ericsson 1992). There is at present no general agreement on the mechanism involved in the creation of the flow asymmetry.

Bird (1969) and Polhamus (1971) reported that initially symmetric leading-edge vortices over slender delta wings became asymmetric at some high angle of attack before vortex breakdown occurred on the wing. However, Stahl, Mahmood & Asghar (1992) revealed that no strongly asymmetric vortex flow was observed before vortex breakdown occurred on the wing in their water tunnel and wind tunnel experiments, and pointed out that the earlier observed onset of vortex asymmetry by Bird (1969) was possibly related to different shapes of the leading edge of the delta wing models. The flat-plate wing model of Stahl *et al.* (1992) has sharp edges, while the flat-plate wing model of Bird (1969) has rounded leading edges. Stahl *et al.* conjectured that near the apex Bird's wing probably had the shape of a more or less thick elliptic cone rather than a thin flat-plate wing. However, Lim, Lua & Luo (2001) showed that the shape near the apex may not be wholly responsible for the vortex asymmetry, with a water tunnel test of flat-plate wings of ogive-shaped planform with different tip and edge geometries, and that the edge geometry also played a crucial role. Ericsson (1992) claims that the vortex asymmetry observed by Shanks (1963) over slender flat-plate wings was probably caused by the asymmetric reattachment of the leading-edge separated flow on the leeward side of Shanks' models. There was a centreline spline mounted on the leeward side of the flat-plate delta wing model of Shanks. Ericsson argued: "The reattaching flow cannot find a stable stagnation point on the top of the centerline spline. As a result, the stagnation point move to one side of the centerline spline, forcing an asymmetry into the cross flow separation geometry, resulting in asymmetric leading-edge vortices."

It was found that the leeward side vortex flow asymmetry over bodies of revolution could be suppressed by means of a fin between the vortices (Stahl 1990; Ng 1990) or by flattening the nose into an elliptic cross-section (Edwards 1978).

Using numerical methods and the vortex line and vortex sheet models of inviscid and incompressible flow Dyer, Fiddes & Smith (1982) and Fiddes & Williams (1989) found asymmetric solutions as well as symmetric solutions for the vortex flow over slender conical bodies even though the separation lines were postulated to be symmetric. These and many other numerical investigations suggest that the appearance of vortex asymmetry is an inviscid phenomenon (for example Lowson & Ponton 1992; Fiddes 1980).

Much work has been focused on experimental observation or numerical computation of the vortex motions behind slender bodies. There are, however, few analytical stability studies on such vortex systems. Using an inviscid incompressible model, Föppl (1913) showed analytically that the vortex pair behind a circular cylinder can be stationary and is unstable to small anti-symmetric perturbations. Smith & Clark (1975) showed that a vortex pair behind a two-dimensional flat plate cannot be stationary. In the three-dimensional flow, Huang & Chow (1996) showed by an analytical method that the vortex pair over a slender flat-plate delta wing can be stationary and is stable to small perturbations for angles of attack up to about two times the semi-apex angle of the wing. The present paper presents general stability analyses of vortices in two dimensions and those over slender conical bodies in three dimensions. A number of practical examples are studied and results compared with experimental data wherever available.

Föppl's (1913) stability analysis of a symmetric vortex pair behind a circular cylinder is a classic result that has been cited by many authors including Lamb (1932), Milne-Thomson (1968), Goldstein (1938), and Saffman (1992, p. 43). Föppl's problem is revisited here, which leads to the derivation of a general stability condition for vortices in two dimensions. This condition involves only the evaluation of the divergence and Jacobian of a vortex velocity field and, therefore, can be easily tested either analytically or by numerical computation when analytical expressions are difficult or impossible to obtain. Computational results using finite differences are validated for the circular cylinder case where analytic solutions are available. The new stability condition is then used to study the stability of a pair of vortices behind a circular cylinder with a splitter plate. It is found that there is a minimum plate length that makes the vortices neutrally stable under anti-symmetric perturbations. The stationary positions and stability of a pair of vortices behind an elliptical cylinder is also investigated.

A conical flow theory is then presented by which the two-dimensional stability condition can be made use of in the study of three-dimensional symmetric vortices over slender conical bodies at high angles of attack. This theory along with the two-dimensional vortex stability condition are subsequently applied to investigate the absolute (temporal) stability of initially symmetric vortex flows over slender circular cones and highly swept flat-plate delta wings with and without vertical fins, and slender elliptic cones of various eccentricities. Results are compared with experimental data.

Zilliac *et al.* (1991), Degani & Tobak (1992), and Levy *et al.* (1996) argue, based on experimental and computational results, that a convective instability is the preferred mechanism for vortex asymmetry of the flow past long cylindrical bodies with conical or ogive front ends. Small disturbances due to geometric imperfections at the nose become amplified as the flow moves downstream in space. Such a spatial instability where disturbances grow in one spatial direction is distinguished from the absolute type of instability discussed in this paper where the growth or decay of disturbances are described in temporal form. In its strict sense, the absolute type of stability presented in this paper should be viewed as a necessary condition for the existence of stable conical symmetric vortices.

2. Stability of vortices in two dimensions

2.1. *Vortices behind a circular cylinder*

Föppl (1913) studied the stability of a pair of vortices behind a circular cylinder of unit radius in a uniform inviscid incompressible stream of velocity U as shown in figure 1. Following Föppl's notation, the pair of vortices are assumed to be at $\zeta_0 = \xi_0 + \mathrm{i}\eta_0$ and $\overline{\zeta}_0 = \xi_0 - \mathrm{i}\eta_0$ in the complex domain. The complex velocity of the flow field can be found by placing two image vortices inside the cylinder and using the principle of superposition as follows:

$$u - \mathrm{i}v = U\left(1 - \frac{1}{\zeta^2}\right) + \frac{\mathrm{i}\Gamma}{2\pi}\left[\frac{1}{\zeta - \zeta_0} + \frac{1}{\zeta - 1/\zeta_0} - \frac{1}{\zeta - \overline{\zeta_0}} - \frac{1}{\zeta - 1/\overline{\zeta_0}}\right], \quad (2.1)$$

where Γ is the strength (circulation) of the vortex and the cylinder radius is assumed to be 1. In an inviscid flow, a concentrated vortex will move with the local flow velocity. This velocity of the vortex at ζ_0 can be found by removing the self-induced velocity term due to the vortex itself. This is justified because a point vortex should be viewed as the limit of a Rankine vortex filament with an infinitesimally small core cross-section (see, for example, Saffman 1992, p. 22). At the centre of the vortex core,

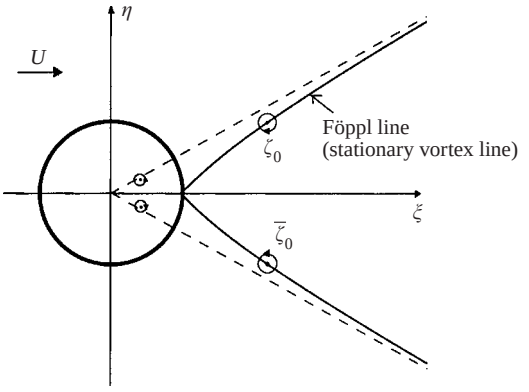

FIGURE 1. Vortices behind a circular cylinder and the Föppl line.

the velocity induced by the vortex itself is zero. For clarity, the subscript 0 is dropped hereafter. Thus, the flow velocity at the centre of the vortex whose location is at $\zeta = \xi + \mathrm{i}\eta$ is

$$u - \mathrm{i}v = U\left(1 - \frac{1}{\zeta^2}\right) + \frac{\mathrm{i}\Gamma}{2\pi}\left[\frac{1}{\zeta - 1/\zeta} - \frac{1}{\zeta - \overline{\zeta}} - \frac{1}{\zeta - 1/\overline{\zeta}}\right]. \tag{2.2}$$

It must be pointed out that the above velocity field is no longer the original velocity field of the flow represented by (2.1). The velocity field given by (2.1) must be divergence free since it represents an incompressible flow. The velocity field represented by (2.2), however, stands for the velocity at which a vortex placed in the flow field will move as a function of its position. Notice also that as ζ changes, the positions of other vortices including the vortex that pairs with the vortex under consideration and the image vortices of the pair will also move to satisfy the symmetry requirement and the wall boundary conditions. Consequently, the velocity field represented by (2.2) should not be taken without proof to be necessarily divergence free. For convenience, we will call it the *vortex velocity* field in this paper. More discussions on this are to follow in the next section.

For the vortices to be stationary ζ cannot be allowed to have arbitrary values since the flow velocity at ζ must be zero. By setting u and v in (2.2) to zero, it is found that any pair of stationary vortices must be located on the curves $\eta_0 = \pm(r_0^2 - 1)/2r_0$, where $r_0 = (\xi_0^2 + \eta_0^2)^{1/2}$. These curves are called Föppl lines (see solid lines in figure 1). Points on the Föppl lines are called stationary points. Vortices located at these points will not move.

The question of stability arises when vortices are slightly perturbed from these stationary points. Föppl studied this problem by decomposing any arbitrary such perturbation into a symmetric and an anti-symmetric perturbation. He found that the vortices were stable for symmetric perturbations, but unstable for anti-symmetric perturbations. Unfortunately, his analysis on the symmetric perturbations was flawed. On re-examination of the problem, the authors found that the vortices are only neutrally stable for symmetric perturbations, as reported in a conference presentation (Cai, Liu & Luo 2001*a*). It was brought to the authors' attention by an anonymous reviewer of this paper that in Smith (1973) a similar analysis had been performed and the above mentioned error in Föppl's paper corrected. Tang & Aubry (1997) also discussed Föppl's problem from a dynamical system point of view. It is interesting

to note that Lamb (1932), in his classical book, cited only Föppl's result on anti-symmetric perturbations when discussing Föppl's (1913) paper; so did Saffman (1992, p. 43) in his book. Perhaps, they too had suspected Föppl's analysis on the symmetric perturbations. The readers are referred to Smith (1973) or Cai *et al.* (2001*a*) for details regarding the correction of Föppl's analysis. The next subsection focuses on the derivation and application of a new generalized stability condition for the motion of a vortex or a group of vortices.

2.2. *A general stability condition*

Consider a system of vortices in a two-dimensional flow. Assume one of the vortices in the system is located at (x, y). As this vortex is moved in the physical plane, other vortices in the system are assumed to move according to a given mode of motion, for instance the symmetric or anti-symmetric mode of motion in the above subsection, subject to given boundary conditions. The starting point for the general stability condition to be discussed below is that given the flow boundary conditions and the mode of vortex motion, one has already obtained, similar to (2.2) for the Föppl problem, the *vortex velocity* (u, v) for the vortex under consideration, i.e. the velocity at which the vortex will move as a function of its location (x, y). The stationary points (x_0, y_0) for the vortex can be found by setting $u(x, y) = 0$ and $v(x, y) = 0$. When the vortex is perturbed from its stationary point (x_0, y_0) and then released, its motion is assumed to follow the vortex velocity (u, v). Let Δx and Δy denote its small displacement from the stationary point. By expanding (u, v) around (x_0, y_0), we find to first order

$$\frac{\mathrm{d}}{\mathrm{d}t}\begin{bmatrix}\Delta x\\ \Delta y\end{bmatrix} = \begin{bmatrix}u\\ v\end{bmatrix} = \begin{bmatrix}\left(\dfrac{\partial u}{\partial x}\right)_0 & \left(\dfrac{\partial u}{\partial y}\right)_0\\ \left(\dfrac{\partial v}{\partial x}\right)_0 & \left(\dfrac{\partial v}{\partial y}\right)_0\end{bmatrix}\begin{bmatrix}\Delta x\\ \Delta y\end{bmatrix}, \tag{2.3}$$

where the subscript 0 denotes values at the stationary point: (x_0, y_0). Define the Jacobian and divergence of the vortex velocity field $\boldsymbol{q} = (u, v)$:

$$J = \begin{vmatrix}\dfrac{\partial u}{\partial x} & \dfrac{\partial u}{\partial y}\\ \dfrac{\partial v}{\partial x} & \dfrac{\partial v}{\partial y}\end{vmatrix}, \quad D = \nabla\cdot\boldsymbol{q} = \frac{\partial u}{\partial x} + \frac{\partial v}{\partial y}. \tag{2.4}$$

It can be easily shown that the eigenvalues of the coefficient matrix in (2.3) are

$$\lambda_{1,2} = \tfrac{1}{2}\left[D_0 \pm \left(D_0^2 - 4J_0\right)^{1/2}\right]. \tag{2.5}$$

The stability condition for the vortex motion may then be summarized as in table 1 based on whether $\lambda_{1,2}$ will yield growing solutions of Δx or Δy.

For the circular cylinder problem in the previous section, the analytical form of $u(x, y)$ and $v(x, y)$ is relatively simple so that both the stationary points and the stability conditions can be found analytically. For more complex problems, such as the flow over a circular cylinder with a splitter plate and over ellipses, and also analyses of three-dimensional problems to be presented later in this paper, a numerical search for the stationary points and evaluation of the stability conditions may be more convenient or necessary. A simple bisecting root-finding algorithm and the standard fourth-order central finite-difference formula are used in this paper.

	D_0	J_0	Comment
Stable	< 0	> 0	
Neutral	< 0	$= 0$	Non-oscillating
	$= 0$	$= 0$	Non-oscillating
	$= 0$	> 0	Oscillating
Unstable	> 0	any	
	any	< 0	

TABLE 1. Stability condition for vortex motion.

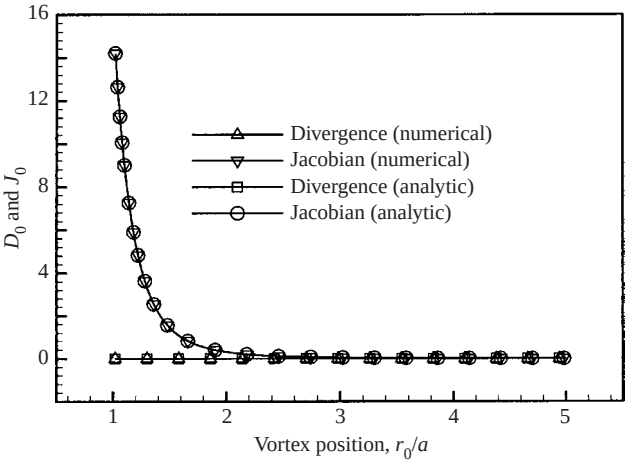

FIGURE 2. Divergence and Jacobian vs. vortex position under symmetric perturbations, circular cylinder case.

Föppl considered the stability of the vortices under symmetric and anti-symmetric perturbations. It is useful to point out that in the consideration of stability for a pair of vortices, it is sufficient to consider only symmetric and anti-symmetric modes of perturbations. Any arbitrary displacements of vortex 1 and vortex 2 on the complex domain, $(\Delta Z_1, \Delta Z_2)$, may always be decomposed as the sum of a symmetric perturbation $(\Delta S, \overline{\Delta S})$ and an anti-symmetric perturbation $(\Delta A, -\overline{\Delta A})$, where $\Delta S = (\Delta Z_1 + \overline{\Delta Z_2})/2$ and $\Delta A = (\Delta Z_1 - \overline{\Delta Z_2})/2$.

It is easily verified that the general stability condition listed in table 1 leads to the same particular stability conditions derived by Föppl (1913) and later corrected by Smith (1973) for the circular cylinder problem. As an example and a means of validating our computational method, numerical computations are performed and compared with the analytical results for the circular cylinder problem. Figures 2 and 3 show numerical and analytical values of D_0 and J_0 versus vortex position r_0/a (a is the radius of the circular cylinder) for the symmetric and anti-symmetric perturbations, respectively. For simplicity, D_0 and J_0 here and from this point on denote the dimensionless quantities $D_0 a/U$ and $J_0 a^2/U^2$, respectively. The computational results are indistinguishable from the analytical values. Clearly, the divergence D_0 for both the symmetric and anti-symmetric perturbations is zero. For the case of symmetric perturbations shown in figure 2, it is found that $J_0 > 0$, which indicates that the

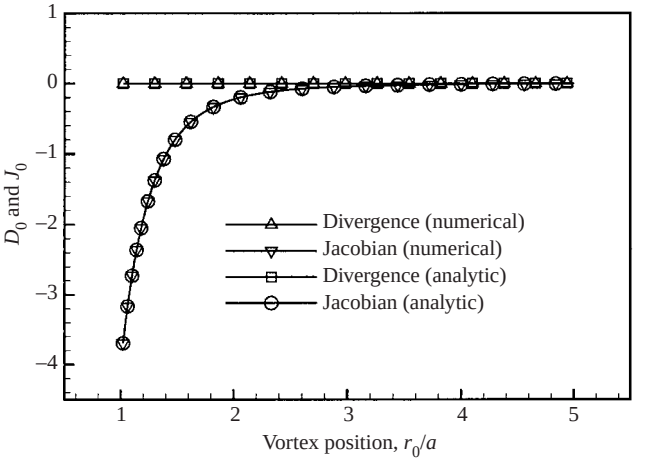

FIGURE 3. Divergence and Jacobian vs. vortex position under anti-symmetric perturbations, circular cylinder case.

vortices are in a neutrally stable state with an oscillatory motion near the stationary points. The oscillation attenuates as the vortices move farther from the cylinder. For the anti-symmetric perturbations shown in figure 3, it is found that $J_0 < 0$, thus the vortices are always unstable. The vortices are more unstable when they are close to the cylinder and gradually approach neutral stability as they move away from the cylinder.

It is noted again at this point that the vortex velocity functions $u(x, y)$ and $v(x, y)$ considered here are not the original incompressible velocity field. They represent the velocity at which a vortex in the flow field will move when its spatial location is at (x, y). As pointed out in the discussions following (2.2), this vortex velocity field, in general, may not be divergence free. It is interesting to find, however, that both the analytic and the computational results shown above for the symmetric vortex pair of the Föppl problem give zero divergence of the vortex velocity field at any stationary point (x_0, y_0) of the vortex, i.e. $D_0 = 0$ for both the symmetric and the anti-symmetric perturbations. It is observed numerically in the following subsections and proven in the Appendix that this property is true for any two-dimensional flow fields that are obtained from the circular cylinder flow through a series of conformal mappings if the vortex system is initially placed symmetrically.† Thus, we conclude that *a symmetric vortex pair in any two-dimensional incompressible flow is either unstable or neutrally stable, but never absolutely stable*. It is easily verified, however, that $D_0 \neq 0$ if the vortex pair is not symmetrically placed as in the Föppl problem, which is of significance in the study of asymmetric vortices. In addition, $D_0 \neq 0$ when the stability analysis is extended to treat three-dimensional problems as will be shown later in the paper.

2.3. *Vortices behind a circular cylinder with a rear splitter*

In this section, the analysis is extended to include a splitter plate at the rear end of a circular cylinder of radius a, where the height of the splitter plate h is measured

† This property was conjectured to be true in the original manuscript of this paper. The authors completed the proof in the Appendix based on a lead suggested by an anonymous reviewer of the manuscript.

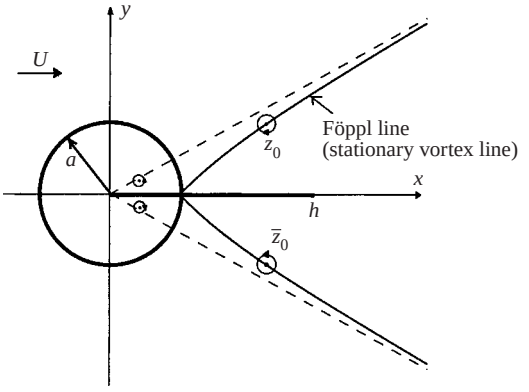

FIGURE 4. Circular cylinder with a rear splitter plate.

from the origin, i.e. the end point of the plate is at $x = h$ (see figure 4). In a three-dimensional situation, this corresponds to the case of having a vertical fin attached to a body of revolution. Since a splitter plate has no effect on the flow so long as the flow is symmetric, the result for the circular cylinder under symmetric perturbations remains unchanged for the case with a splitter plate, that is, the vortices will be neutrally stable. The splitter plate, however, will affect the flow under anti-symmetric perturbations. Intuitively, it reduces the 'communication' between the top and bottom vortices. It is interesting to see whether this reduction in 'communication' may reduce the instability due to anti-symmetric perturbations that exists in the circular cylinder case, and if so, whether there is a minimum length of the splitter plate that makes the vortices stable or neutrally stable.

The velocity field around a circular cylinder of radius a with the splitter plate in the complex plane $Z = x + \mathrm{i}y$ can be easily found by using a conformal mapping from the flow past a circular cylinder of radius σ without the splitter plate in the plane $\zeta = \xi + \mathrm{i}\eta$. That is

$$\frac{1}{2}\left(Z + \frac{a^2}{Z}\right) - X_m = \frac{1}{2}\left(\zeta + \frac{\sigma^2}{\zeta}\right), \tag{2.6}$$

where $X_m = (a-h)^2/4h$ and $\sigma = (a+h)^2/4h$.

Suppose the symmetric stationary vortices undergo small arbitrary displacements, i.e. Z_0 and $\overline{Z}_0$ change to Z_1 and Z_2, respectively. The circulation of the vortices Γ may be assumed unchanged for a short period of time immediately after the small displacement. When Z_1 and Z_2 are not symmetric to the real axis x, a vortex will be shed from the sharp edge of the splitter plate to satisfy the finite velocity condition at the sharp edge. Under small perturbations, however, the strength of this vortex is of the order $\Gamma|\Delta Z|/a$, much weaker than that of the original symmetric vortex pair. Therefore, the shed vortex can be ignored in the following stability analysis for the anti-symmetric perturbation.

The vortex velocity at Z_1 is obtained by a limiting process (see Rossow 1978):

$$u - \mathrm{i}v = \left[U\left(1 - \frac{\sigma^2}{\zeta_1^2}\right) + \frac{\mathrm{i}\Gamma}{2\pi}\left(-\frac{1}{\zeta_1 - \sigma^2/\overline{\zeta_1}} - \frac{1}{\zeta_1 - \zeta_2} + \frac{1}{\zeta_1 - \sigma^2/\overline{\zeta_2}}\right)\right]\left(\frac{\mathrm{d}\zeta}{\mathrm{d}Z}\right)_1 - \frac{\mathrm{i}\Gamma}{4\pi}\left(\frac{\mathrm{d}^2 Z}{\mathrm{d}\zeta^2}\right)_1\left(\frac{\mathrm{d}\zeta}{\mathrm{d}Z}\right)_1^2, \tag{2.7}$$

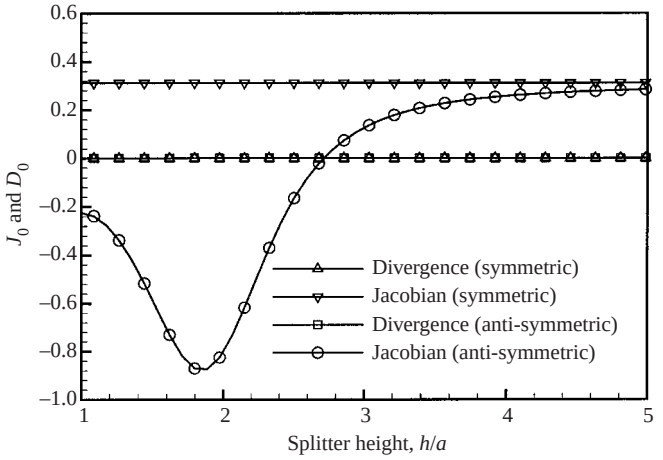

FIGURE 5. Divergence and Jacobian vs. height of splitter plate for circular cylinder with a splitter plate, $r_0/a = 2$, $\theta_0 = 53.4°$.

where $(\mathrm{d}\zeta/\mathrm{d}Z)_1$ and $(\mathrm{d}^2Z/\mathrm{d}\zeta^2)_1$ denote values at $\zeta = \zeta_1$ or $Z = Z_1$, which can be easily obtained by differentiating (2.6). The symmetric stationary points (x_0, y_0) of the vortices can be found by setting the above equation to zero for $Z_1 = Z_0$ and $Z_2 = \overline{Z_0}$.

The stability conditions in § 2.2 are then applied to (2.7) in terms of $Z = Z_1$. The perturbation is decomposed into symmetric and anti-symmetric perturbations,

$$\text{symmetric:}\quad Z_1 = Z_0 + \Delta Z = Z, \quad Z_2 = \overline{Z_0} + \overline{\Delta Z} = \overline{Z}, \tag{2.8}$$

$$\text{anti-symmetric:}\quad Z_1 = Z_0 + \Delta Z = Z, \quad Z_2 = \overline{Z_0} - \overline{\Delta Z} = 2\overline{Z_0} - \overline{Z}, \tag{2.9}$$

where $\Delta Z = \Delta x + \mathrm{i}\Delta y$ is the perturbation, and $|\Delta x| \ll a$, $|\Delta y| \ll a$. The strength of the vortices is kept constant during the perturbation because the perturbations are considered small and instant. After inserting (2.8) and (2.9) into (2.7), we can then easily calculate the divergence and Jacobian of the vortex velocity field (u, v) either analytically or numerically.

For this example, fourth-order-accurate finite-difference formulae are used in evaluating D_0 and J_0 with 64-bit arithmetic for extra accuracy. Notice that the stationary points of the vortices for this case remain on the same Föppl line as that for the circular cylinder in § 2.1. We consider the particular case where the stationary point is at $x_0/a = 55^{1/2}/4$, $y_0/a = 3/4$, and $r_0/a = 2$. The corresponding vortex strength at this point is $\Gamma/Ua = 45\pi/16$. The corresponding symmetric separation point is at $\theta_0 = 53.4°$. The separation angle θ_0 is measured anti-clockwise from the rear end of the cylinder. The separation condition on the body used here is that the velocity at the separation point vanishes and the velocities on both sides of the separation point are towards the point.

As mentioned at the end of the previous subsection, the divergence of the vortex velocity field for this case is zero. Direct numerical computations show values of the order of 10^{-20} for $U = 1$ and $a = 1$. Therefore, the stability of this case depends on the sign of J_0. The vortices are unstable when $J_0 < 0$, and neutrally stable when $J_0 \geqslant 0$. The relative strength of stability or instability can be inferred from the size of J_0. Figure 5 shows the calculated divergence and Jacobian at the above x_0 and y_0 versus height of the splitter plate. Clearly, the divergence is zero for both symmetric and anti-symmetric perturbations. The symmetric result should be independent of the

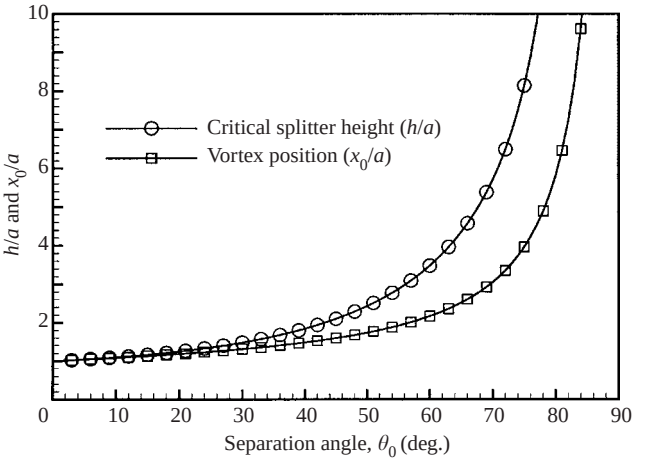

FIGURE 6. Vortex position and critical height of splitter plate as function of separation angle for a circular cylinder with a splitter plate.

height of the splitter plate, which is confirmed by the constant positive J_0 shown in figure 5.

For the anti-symmetric perturbations, J_0 is less than zero for splitter plates that are shorter than approximately 1.7 times the radius of the cylinder, i.e. $h/a < 2.7$. The vortices become neutrally stable when the length of the splitter plate increases beyond that critical value. As the length of the splitter plate goes to infinity, J_0 approaches the value of the symmetric perturbation because the splitter plate restrains the asymmetric motion of the vortices. Note also that, as the length of the splitter plate increases from zero, the vortices initially become less stable (J_0 decreases) until the plate length reaches about 0.8 times the radius of the circular cylinder. At that point the value of J_0 begins to increase. It is not until the length of the plate reaches about $1.4a$ that the addition of the splitter plate enhances the stability compared to without the splitter plate. In other words, when the splitter plate is not long enough, it has an opposite effect, i.e. the addition of the splitter plate makes the symmetric stationary vortex pair more unstable under anti-symmetric perturbations. No two-dimensional experimental data have been found yet by the authors to support this finding. However, similar effects are predicted and shown to agree with known experimental observations for three-dimensional flows over circular cones presented later in the paper.

Figure 6 shows the vortex position x_0/a and the critical height h/a of the splitter plate as a function of the separation angle θ_0. Both h/a and x_0/a increase with an increase of θ_0, and the critical height h/a is always greater than x_0/a. Physically, the splitter plate must extend further downstream than the vortices in order to cut off the 'communication' between the two vortices as the vortices move away from the cylinder. This agrees with the experimental results of Roshko (1961), which showed that the main effect of the splitter plate with $h/a = 6.3$ and θ_0 about 75° is the suppression of the alternating vortex shedding and removal of the peak frequency in the spectrum. Figure 6 predicts that the critical height of the splitter plate is $h/a = 8.1412$ for $\theta_0 = 75°$. The above results provide guidance in the choice of the height of the splitter plate required to suppress the alternating vortex shedding behind the circular cylinder.

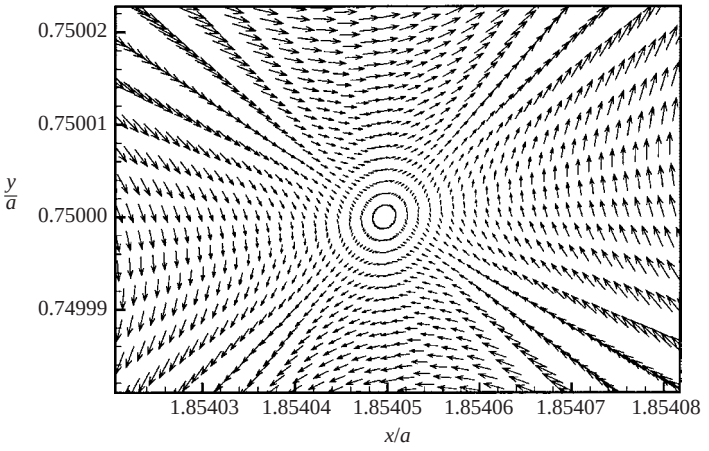

FIGURE 7. Velocity of vortex under anti-symmetric perturbations for the flow over a circular cylinder with a splitter plate, $h/a = 2$, $r_0/a = 2$, $\theta_0 = 53.4°$ (unstable case).

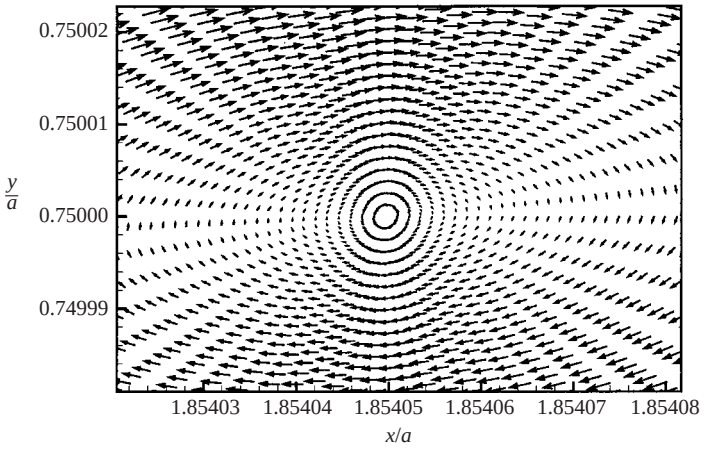

FIGURE 8. As figure 7 but for $h/a = 4$ (neutrally stable case).

Although the formulae to calculate the vortex velocity for this case are different and more complex than those for the pure circular cylinder case, it is expected that the results for this case must reduce to those of the pure circular cylinder case as the length of the splitter plate becomes zero. Indeed, from figure 5, the calculated value of J_0 is 0.311523 for symmetric perturbations and -0.223630 for anti-symmetric perturbations when $h/a = 1$, which are identical to the analytical values for the circular cylinder to the 6th significant digit.

In order to appreciate the physical meaning of the stability conditions in terms of D_0 and J_0, figures 7 and 8 show the vortex velocity fields for anti-symmetric perturbations for two cases with plate heights $h/a = 2$ and $h/a = 4$, respectively. It is known from figure 5 that the former is unstable and the latter is neutrally stable. Clearly, figures 7 and 8 show a zero vortex velocity at the stationary vortex point under consideration. Since the divergence of the velocity field $D_0 = 0$ at the stationary point, some velocities must move out from this stationary point if others move inwards, which is the case when $J_0 < 0$. It is the existence of the diverging

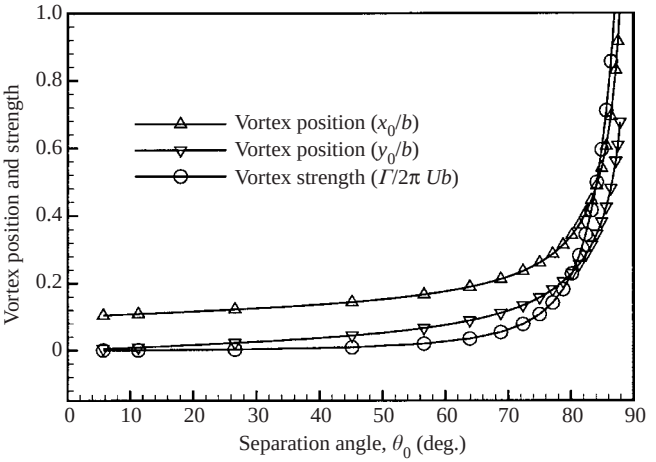

FIGURE 9. Vortex position and strength vs. separation angle for an elliptic cylinder, $\tau = 0.1$.

velocities that leads to instability. For the case with $h/a = 4$, the splitter plate is long enough to make the vortex neutrally stable under anti-symmetric perturbations. Since D_0 is still zero, $J_0 > 0$ indicates that the velocity vectors form circles around the stationary point as is confirmed by figure 8. In this case, the vortex is in an oscillatory, neutrally stable condition around the stationary point.

As proven in the Appendix, the divergence of the velocity field of the motion of a vortex in a symmetric vortex configuration placed in a two-dimensional incompressible flow is always zero at its stationary points. Therefore, vortices in a two-dimensional incompressible flow can be at best neutrally stable. However, if D_0 could be less than zero, there would exist the possibility that the vortex velocity vectors may all be drawn towards the stationary point when $J_0 > 0$, leading to a stable vortex configuration. On the other hand, when $D_0 > 0$, the vortex must be unstable regardless of the value of J_0 because of the fact that some velocity vectors must leave the stationary point when the divergence is positive. Such situations exist in three dimensions as will be shown later.

2.4. *Vortices behind an elliptic cylinder*

The circular cylinder in figure 4 is in this case replaced by an ellipse with one of its axes placed perpendicular to the free-stream flow and the other along the free-stream flow. The lengths of these two axes are assumed to be $2b$ and $2c$, respectively. The thickness ratio of the elliptic cylinder is defined as $\tau = c/b$. The two vortices behind the elliptic cylinder are at $Z_0 = x_0 + \mathrm{i}y_0$ and $\overline{Z}_0 = x_0 - \mathrm{i}y_0$.

The vortex velocity field for this case is given by (2.7) with U replaced by $U/2$ and $\sigma = 1$. However, the transformation from ζ to Z is now $Z = (\zeta + \lambda/\zeta)/2$, where $c = (1 + \lambda)/2$ and $b = (1 - \lambda)/2$.

Figure 9 shows the stationary position and the strength of the vortices versus the flow separation angle on the surface of the elliptic cylinder for $\tau = 0.1$. Again, the separation angle is measured anti-clockwise from the rear stagnation point of the cylinder. It is found for this case that the stationary vortices must be placed infinitely far away from the cylinder as the separation point on the cylinder moves towards the crest, i.e. when θ_0 approaches 90°. This is true for any value of τ. This means that it is not possible to find stationary points of the vortices when separation occurs at the top and bottom extremes of the elliptic cylinder. This agrees with the finding by

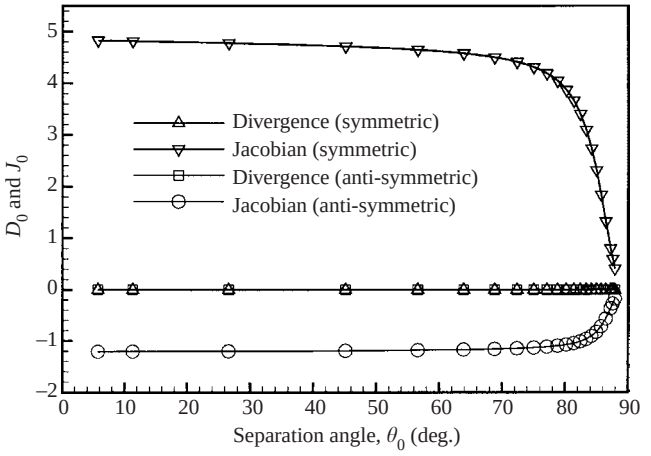

FIGURE 10. Divergence and Jacobian vs. separation angle for an elliptic cylinder, $\tau = 0.1$.

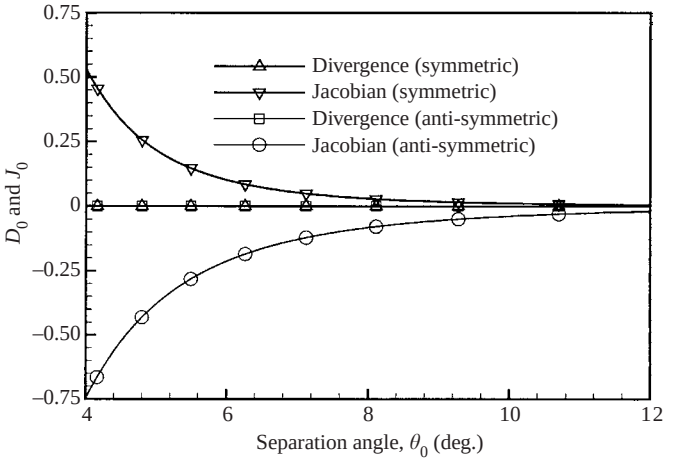

FIGURE 11. Divergence and Jacobian vs. separation angle for an elliptic cylinder, $\tau = 6.0$.

Smith & Clark (1975) that no stationary points exist for a flat plate normal to the flow where separation must occur at the ends of the plate, i.e. $\theta_0 = 90°$, in order to satisfy the Kutta condition. The ellipse approaches a vertical flat plate as $\tau \to 0$.

Figure 10 shows the D_0 and J_0 for this case. It is noticed again that D_0 is zero for both the symmetric and anti-symmetric perturbations. Therefore, the vortex system is at most neutrally stable. For anti-symmetric perturbations, J_0 is always less than zero. Therefore, the vortices are unstable to small anti-symmetric perturbations. On the other hand, J_0 is always greater than zero for symmetric perturbations, and thus the vortices are neutrally stable to small symmetric perturbations. These conclusions for an elliptic cylinder are qualitatively identical to those for the circular cylinder case.

Figure 11 shows the result for an elliptic cylinder with $\tau = 6$. It is seen that the stationary symmetric vortex pair is unstable to small anti-symmetric perturbations, and thus may lead to possible asymmetric configurations or asymmetric vortex shedding. This agrees with the wind-tunnel test results (Bradshaw 1970; also Van

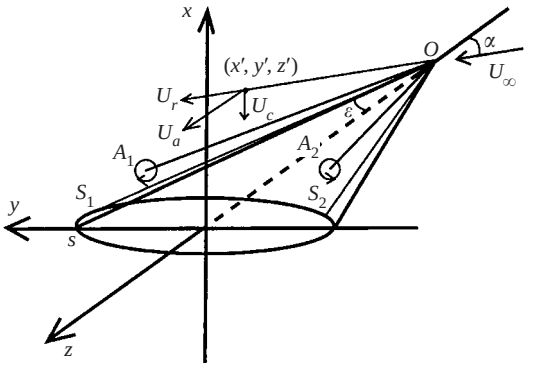

FIGURE 12. Slender conical body and separation vortices.

Dyke 1982, figure 32, p. 24) at a Reynolds number 4000 based on $2c$. The experimental results show that a laminar boundary layer separates at $\theta_0 \approx 8^\circ$ and sheds alternating vortices.

3. The vortex velocity for slender conical bodies

This section describes the assumptions and method to reduce the problem of the three-dimensional potential flow over slender conical bodies to a two-dimensional problem in the conical coordinate system so that the stability condition derived in the above section can be readily applied.

Consider the flow past a slender conical body of an arbitrary symmetric cross-section at an angle of attack α and zero sideslip as shown in figure 12. The plane of symmetry of the body Oxz coincides with the incidence plane of the flow. The body may have a slender triangular flat-plate fin on the top and/or the lower surface of the body in the plane of symmetry. The flow separates from the body surface along symmetric separation lines with respect to the symmetry plane of the body. The flow is assumed to be steady, inviscid, incompressible and conical.

Under the conical flow assumption, the separation lines OS_1 and OS_2 are assumed to be rays starting from the body apex O as shown in figure 12. In a real flow, a pair of vortex sheets erupts from the separation lines OS_1 and OS_2. The sheets extend along the leeward side of the body and then roll tightly into two concentrated vortices at a certain distance from the body. The distributed vortex sheets that connect the separation lines and the two concentrated vortices are neglected since their strength is in general much smaller than that of the two concentrated vortices. Such a simplified model was used by Legendre (1953) and Adams (1953) and also Huang & Chow (1996). As pointed out by Huang & Chow (1996), neglect of the distributed vortex sheets causes errors in the calculation of the lift over the body but serves adequately in a stability analysis. The two concentrated symmetric vortices can be approximated as a pair of vortex lines OA_1 and OA_2, which are also assumed to be rays from the body apex O under the conical flow assumption.

The inviscid incompressible flow considered in the above model is potential except at the centres of the isolated vortices. The governing equation for the velocity potential is the three-dimensional Laplace equation with zero normal flow velocity on the body surface as the boundary condition. By the principle of superposition, the flow around the body can be obtained by solving the following two flow problems: (i) the flow

due to the normal component of the free-stream velocity; and (ii) the flow due to the axial component of the free-stream velocity, both subject to zero normal velocity at the wall. We denote the velocity field of the first problem by $\boldsymbol{U}_1$ and that of the second problem by $\boldsymbol{U}_2$.

In the first problem, the slender body is placed normal to the cross-flow component $U_n = U_\infty \sin\alpha$. Since the body is assumed to be slender, the velocity in the z-direction due to three-dimensional effects can be neglected. The flow in each cross-section at z may then be regarded as a two-dimensional flow across the local cross-sectional profile governed by the two-dimensional Laplace equation with zero normal velocity at the wall. A solution to this two-dimensional velocity field can be obtained by conformal mapping or other analytical or numerical methods. For simple profiles such as circles and ellipses with or without fins, $\boldsymbol{U}_1$ can be easily obtained by conformal mapping as discussed in the previous section.

The second problem, that for $\boldsymbol{U}_2$, corresponds to the flow past a conical body with a free-stream velocity $U_a = U_\infty \cos\alpha$ and zero angle of attack. As shown in figure 12, consider the description of the same flow in two different but related coordinate systems. The first is the conventional orthogonal system (x, y, z). The second is the nonorthogonal conical coordinate system $(x', y', r') = (x/s, y/s, z)$, where s is the semi-span of the body at z in the (x, y)-plane, which is related to the semi-apex angle of the body ε by $s = z\tan\varepsilon$. The unit vectors of the two coordinate systems are then related by: $\boldsymbol{e}_{x'} = \boldsymbol{e}_x$, $\boldsymbol{e}_{y'} = \boldsymbol{e}_y$, and $\boldsymbol{e}_{r'} = (x\boldsymbol{e}_x + y\boldsymbol{e}_y + z\boldsymbol{e}_z)/(x^2 + y^2 + z^2)^{1/2}$.

Under the assumption of small perturbations for slender bodies, $\boldsymbol{U}_2$ can be described in the first coordinate system as

$$\boldsymbol{U}_2(x, y, z) = \boldsymbol{U}_p(x, y; z) + U_a\boldsymbol{e}_z, \tag{3.1}$$

where $\boldsymbol{U}_p(x, y; z)$ is a two-dimensional velocity vector in the $(\boldsymbol{e}_x, \boldsymbol{e}_y)$-plane with z being a parameter for each cross-section of the body. By using the transformation between the unit vectors in the two coordinate systems, $\boldsymbol{U}_2$ can be converted to

$$\boldsymbol{U}_2(x, y, z) = \boldsymbol{U}_p(x', y') + \boldsymbol{U}_c(x', y') + u_{r'}(x', y')\boldsymbol{e}_{r'}, \tag{3.2}$$

where

$$u_{r'}(x', y') = U_a(x^2 + y^2 + z^2)^{1/2}/z, \tag{3.3}$$

$$\boldsymbol{U}_c(x', y') = -\frac{U_n}{K}(x'\boldsymbol{e}_{x'} + y'\boldsymbol{e}_{y'}), \tag{3.4}$$

and K is the Sychev similarity parameter (Sychev 1960)

$$K = \tan\alpha/\tan\varepsilon. \tag{3.5}$$

Notice that $\boldsymbol{U}_p$ is now written in (3.2) as functions of x' and y' only due to the conical flow assumption.

The velocity potential for $\boldsymbol{U}_2(x, y, z)$ satisfies the three-dimensional Laplace equation, subject to the boundary condition $\boldsymbol{U}_2 \cdot \boldsymbol{n} = 0$ at the body surface, where $\boldsymbol{n}$ is the normal vector to the surface of the three-dimensional body. Consequently, $\boldsymbol{U}_p$ is a two-dimensional potential flow and can be obtained by solving the two-dimensional Laplace equation in the (x', y')-plane subject to the two-dimensional wall boundary condition

$$\boldsymbol{U}_p(x', y') \cdot \boldsymbol{n}_c = -\boldsymbol{U}_c(x', y') \cdot \boldsymbol{n}_c, \tag{3.6}$$

where $\boldsymbol{n}_c$ is the normal vector to the two-dimensional cross-sectional profile of the body.

The velocity $\boldsymbol{U}_c(x', y')$ represents the flow velocity drawn towards the body axis when the axial flow is decomposed into the velocity along the conical ray and the velocity in the cross-sectional plane. At the surface of the body, the normal component of this velocity must be cancelled by the potential field $\boldsymbol{U}_p$. Physically, $\boldsymbol{U}_p$ represents the displacement effect of a non-zero-thickness body. In the case of a circular cone, the solution for $\boldsymbol{U}_p$ is simply one single point source, which can be written in the complex velocity format as

$$u_p - \mathrm{i}v_p = \frac{U_n a}{KZ}, \tag{3.7}$$

where a is the radius of the cone at z. In the case of the triangular flat-plate wing, $u_p - \mathrm{i}v_p = 0$ since the right-hand side of (3.6) is zero for a zero-thickness flat-plate wing. For more complex geometries, $\boldsymbol{U}_p$ can be obtained by a singularity method, e.g. by distributing point sources within the body contour. The complex velocity at the point $Z = x + \mathrm{i}y$ due to N point sources at $Z_j = x_j + \mathrm{i}y_j$ can be written as

$$u_p - \mathrm{i}v_p = \frac{1}{2\pi} \sum_{j=1}^{N} \frac{Q_j}{Z - Z_j}, \tag{3.8}$$

where Q_j is the strength of the point sources and $Q_j\,(j = 1, 2, \ldots N)$ are to be determined by N simultaneous equations of the boundary condition on the body contour.

Notice that $\boldsymbol{U}_1$ and $\boldsymbol{U}_p(x, y; z)$ depend only on x' and y'. On superposition, the complete three-dimensional flow field is represented in the non-orthogonal conical coordinate system as

$$\boldsymbol{U}(x', y') = \boldsymbol{V}(x', y') + u_{r'}(x', y')\boldsymbol{e}_{r'}, \tag{3.9}$$

where

$$\boldsymbol{V}(x', y') = \boldsymbol{U}_1(x', y') + \boldsymbol{U}_p(x', y') + \boldsymbol{U}_c(x', y'). \tag{3.10}$$

Notice that $\boldsymbol{V}(x', y')$ is a two-dimensional velocity vector field in the plane $(\boldsymbol{e}_{x'}, \boldsymbol{e}_{y'})$ and the $u_{r'}(x', y')\boldsymbol{e}_{r'}$ term in (3.9) is a velocity component in the ray direction $\boldsymbol{e}_{r'}$ which does not contribute to the flow velocity in the plane $(\boldsymbol{e}_{x'}, \boldsymbol{e}_{y'})$. Consequently, the stability of the flow system can be analysed by studying only the two-dimensional 'flow field' $\boldsymbol{V}(x', y')$ in (3.10). The vortex stability condition listed in table 1 will then readily apply.

4. Analyses of typical slender conical bodies

The above flow model and stability theory are used in this section to analyse the stability of symmetric vortices over a number of typical slender conical bodies. Comparisons with experimental data are made whenever available.

4.1. *Slender circular cones*

A circular cone of semi-apex angle ε at an angle of attack α and no sideslip is considered. Figure 13 shows the circular cross-section of the body at a given distance from the apex, where a is the radius of the circular cross-section, h_W and h_L are the heights of the windward and leeward splitter plates that may be added to the cone. For the discussions in this subsection, h_W and h_L are zero. The separation lines are postulated to be symmetric with respect to the incidence plane Oxz. The position of the separation line OS_1 is specified by the angle θ_0 in the (x, y)-plane measured in

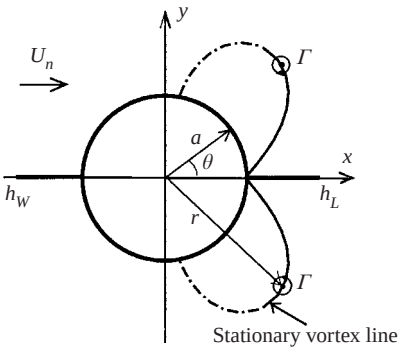

FIGURE 13. Stationary vortex line for a circular cone with or without fins, $K = 5.5591$.

the anti-clockwise direction starting from the leeward side end of the cone. In the cross-flow plane, the initially stationary symmetric vortices of strength Γ are located at Z_1 and Z_2. By the method presented in the proceeding sections, the velocity at any point $Z = x + \mathrm{i}y$ except at Z_1 and Z_2 is given in the complex velocity form

$$u - \mathrm{i}v = U_n\left(1 - \frac{a^2}{Z^2}\right) + \frac{\mathrm{i}\Gamma}{2\pi}\left(\frac{1}{Z - Z_1} - \frac{1}{Z - a^2/\overline{Z_1}} - \frac{1}{Z - Z_2} + \frac{1}{Z - a^2/\overline{Z_2}}\right) + \frac{U_n a}{KZ} - \frac{U_n \overline{Z}}{aK}. \quad (4.1)$$

On the right-hand side of the above equation, the first two terms are the $\boldsymbol{U}_1$ term due to the normal velocity component of the free-stream flow U_n, and the last two terms are $\boldsymbol{U}_p$ and $\boldsymbol{U}_c$ due to the axial velocity component of the freestream flow U_a. The tangential velocity on the body contour is obtained by substituting $Z = a\mathrm{e}^{\mathrm{i}\theta}$ in (4.1).

The velocity at the vortex point Z_1 is obtained by removing the induced velocity term due to the vortex at Z_1 itself, i.e.

$$u - \mathrm{i}v = U_n\left(1 - \frac{a^2}{Z_1^2}\right) + \frac{\mathrm{i}\Gamma}{2\pi}\left(\frac{1}{Z_1 - a^2/\overline{Z_2}} - \frac{1}{Z_1 - Z_2} - \frac{1}{Z_1 - a^2/\overline{Z_1}}\right) + \frac{U_n a}{KZ_1} - \frac{U_n \overline{Z_1}}{aK}. \quad (4.2)$$

The stationary symmetric vortex position Z_0 and the vortex strength Γ are determined by setting the vortex velocity in (4.2) to zero at Z_0 and requiring that the flow velocity given by (4.1) be zero at a separation point $Z = a\mathrm{e}^{\mathrm{i}\theta_0}$ on the wall.

As an example, consider the case of a circular cone with semi-angle $\varepsilon = 8^\circ$ at an angle of attack $\alpha = 38^\circ$, corresponding to $K = 5.5591$. Figure 13 shows a cross-section of the body. The solid lines off the circular body are locations where the two symmetric vortices can be stationary while resulting in a flow field with symmetric separation points on the body surface. As the vortices move away from the rear stagnation point along the stationary path, the vortex strength increases monotonically and the separation angle increases from 0° to about 100°. Further movement along the path results in a flow field that has no separation point on the surface of the circular body. This is marked by the dot-dashed lines in figure 13.

The stationary symmetric vortex positions obtained by the present analytical method for different values of the similarity parameter K and the separation angle $\theta_0 = 34^\circ$ are compared in figure 14 with the numerical solutions given by Dyer

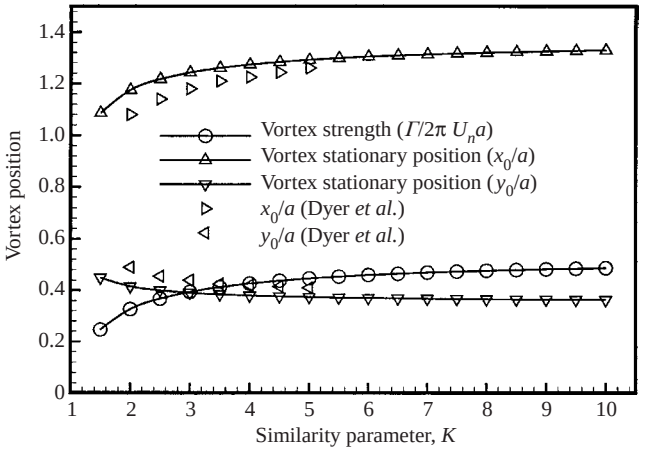

FIGURE 14. Stationary symmetric vortex position for a circular cone, comparison with Dyer *et al.* (1982), $\theta_0 = 34°$.

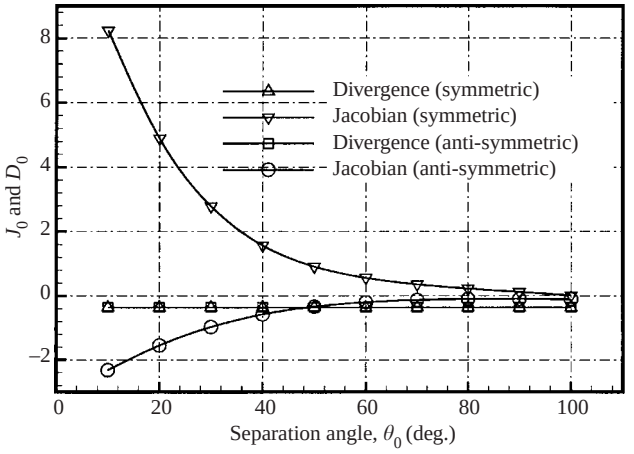

FIGURE 15. Divergence and Jacobian vs. separation angle for a circular cone, $K = 5.5591$.

et al. (1982), who used Bryson's vortex line model for the slender circular cone in an incompressible inviscid flow. The results agree well at large K values. The differences at lower K values may be attributed to the differences in the models used by the two methods. Figure 14 also shows the vortex strength vs. K for this case.

Figure 15 shows the dimensionless divergence D_0 and the dimensionless Jacobian J_0 at (x_0, y_0) versus the separation angle θ_0 for the three-dimensional circular cone case when $K = 5.5591$. For simplicity, D_0 and J_0 in figure 15 and all other figures denote the dimensionless values $D_0 L/U_n$ and $J_0 L^2/U_n^2$, respectively, where L is a length scale. In this case $L = a$. Unlike in the two-dimensional case, D_0 is non-zero for both the symmetric and anti-symmetric perturbations. This non-zero D_0 is produced by $\boldsymbol{U}_c$ in (3.4), which is induced by the axial component U_a of the incoming flow and is valid for all the slender conical bodies. The other terms of the vortex velocity expression (4.2) have no contribution to D_0. Thus, we have $D_0 = -2U_n/aK$, which is always negative. Consequently, a pair of symmetric vortices over a slender conical body are

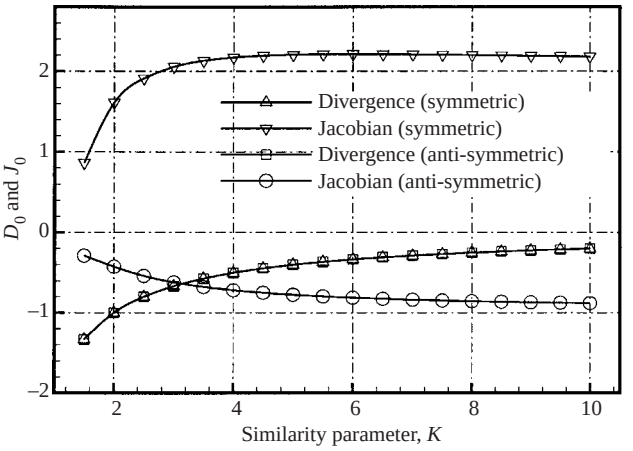

FIGURE 16. Divergence and Jacobian vs. similarity parameter for a circular cone, $\theta_0 = 34°$.

stable, neutrally stable or unstable, when the Jacobian $J_0 > 0$, $J_0 = 0$, or $J_0 < 0$, respectively, according to the stability conditions listed in table 1.

Figure 15 shows that the Jacobian J_0 for symmetric perturbations is always greater than zero and the Jacobian J_0 for anti-symmetric perturbations is always less than zero for $K = 5.5591$, indicating that the symmetric vortices over the circular cone are stable to symmetric perturbations and unstable to anti-symmetric perturbations. Thus, the initially symmetric vortex flow over the slender circular cone tends to become asymmetric. This agrees with the well-known experimental results, e.g. Asghar *et al.* (1994).

The dependence of the vortex stability on the similarity parameter K for a fixed separation position $\theta_0 = 34°$ is shown in figure 16. It is seen that the vortex instability increases monotonically as K increases. For a circular cone of a given apex angle, this means that the asymmetry tendency for the initially symmetric vortex pair increases as the angle of attack α increases.

Figure 14 shows that the vortex coordinates x and y remain close to the conical body. This indicates that the slenderness assumption of the body–vortex combination is good even for large values of K and the separation angle. This is true for all other cases studied in this paper.

4.2. *Slender circular cones with fins*

The two-dimensional analyses in § 2.3 show that adding a flat-plate fin of sufficient length to the rear end of a circular cylinder stabilizes the symmetric vortices behind the circular cylinder under anti-symmetric perturbations. In three dimensions this is equivalent to adding a triangular flat-plate fin on the leeward side of the circular cone in the symmetry plane. In general, a windward side fin of this type may also be added. A cross-section of a circular cone with both the leeward and windward fins corresponds to a two-dimensional circular cylinder of radius a with a leading fin and a trailing fin as shown in figure 13. The two fins are characterized by the heights h_W and h_L measured from the centre of the cylinder. The radius of the circle and the height of the fins must scale linearly with the distance z of the cross-section from the nose of the circular cone. Thus, the ratios h_W/a and h_L/a determine the relative size of the fins and the circular cone.

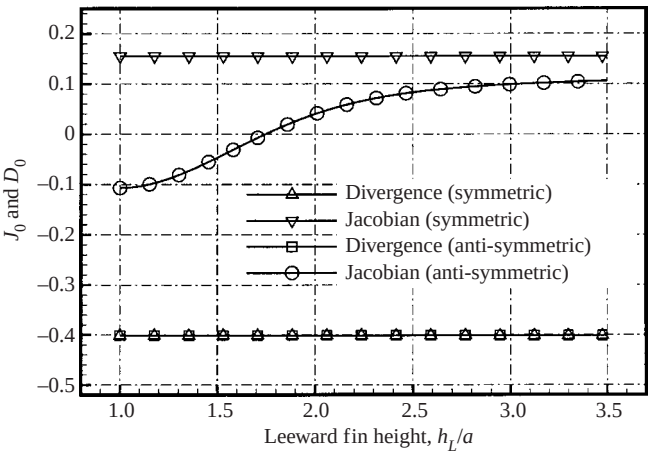

FIGURE 17. Divergence and Jacobian vs. leeward fin height for a circular cone, $K = 4.9822, \theta_0 = 85°, h_W = 0$.

Since the fin is located in the symmetry plane of the body, it has no effect on the symmetric flows. The stationary symmetric vortex position and strength as function of θ_0 are the same as those of the circular cone without the fin. By using the two-dimensional results of § 2.3, the complex velocity at the vortex point Z_1 can be obtained by adding to (2.7) the appropriate three-dimensional terms as follows:

$$u - \mathrm{i}v = \left[U_n(1-\sigma^2/\zeta_1^2) + \frac{\mathrm{i}\Gamma}{2\pi}\left(-\frac{1}{\zeta_1-\zeta_2} - \frac{1}{\zeta_1-\sigma^2/\overline{\zeta_1}} + \frac{1}{\zeta_1-\sigma^2/\overline{\zeta_2}}\right)\right]\left(\frac{\mathrm{d}\zeta}{\mathrm{d}Z}\right)_1 - \frac{\mathrm{i}\Gamma}{4\pi}\left(\frac{\mathrm{d}^2Z}{\mathrm{d}\zeta^2}\right)_1\left(\frac{\mathrm{d}\zeta}{\mathrm{d}Z}\right)_1^2 - \frac{U_n\overline{Z_1}}{aK} + \frac{U_n a}{KZ_1}. \quad (4.3)$$

The conformal mapping relation (2.6) still applies, but the formulas for X_m and σ must be modified to include the windward splitter plate, i.e.

$$X_m = \frac{(a^2+h_L^2)}{4h_L} - \frac{(a^2+h_W^2)}{4h_W}, \quad \sigma = \frac{(a^2+h_L^2)}{4h_L} + \frac{(a^2+h_W^2)}{4h_W}.$$

Asghar *et al.* (1994) gives wind tunnel test results for a circular cone of semi-apex angle $\varepsilon = 8°$ with a leeward fin of $h_L/a = 2.0$ at an angle of attack $\alpha = 35°$ ($K = 4.9822$). The Reynolds number based on the base diameter D is $Re_D = 1.42\times10^5$. The separation angle is estimated to be $85° < \theta_0 < 95°$. The measured circumferential pressure distribution in a cross-section and the distribution of the ratio of side force to normal force along the axis of the circular cone indicate that the flow is asymmetric without the fin but becomes symmetric when the fin is added. The present stability analyses are applied to this experimental case. Figure 17 shows the dependence of D_0 and J_0 on h_L/a with $K = 4.9822$ at $\theta_0 = 85°$. At this separation angle, the vortex flow changes from unstable to stable at a critical fin height $h_L/a = 1.7828$. Similar calculations are performed for $\theta_0 = 95°$ and the critical fin height is found to be $h_L/a = 2.3833$. Considering the uncertainties of the separation angle in the experiment, the present analytical result agrees well with the experimental result by Asghar *et al.* (1994) that a fin of $h_L/a = 2$ largely suppresses the vortex asymmetry that is present on the cone without the fin.

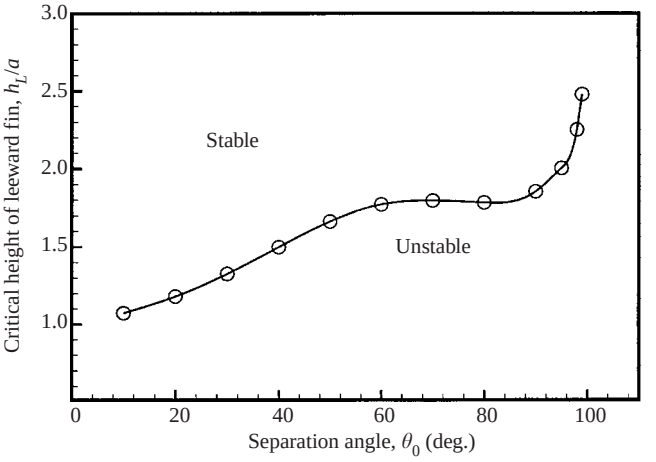

FIGURE 18. Critical fin height vs. separation angle for a circular cone with fin, $K = 5.5591$, $h_W = 0$.

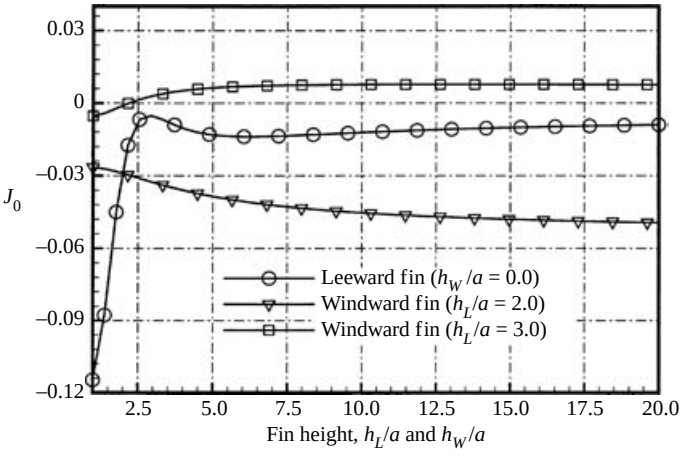

FIGURE 19. Jacobian under anti-symmetric perturbations vs. leeward or windward fin height for a circular cone, $K = 5.5591$, $\theta_0 = 100°$.

Figure 18 shows the dependence of the critical height of the leeward fin on the circular cone on the separation angle θ_0 for $K = 5.5591$. At this value of K, the critical height of the leeward fin increases with θ_0 and increases rapidly when θ_0 approaches 100°.

An additional flat-plate triangular fin on the windward side is needed to suppress the vortex asymmetry when the separation point is at $\theta_0 \geqslant 100°$ and $K = 5.5591$. For this case, again the corresponding divergence D_0 is always negative. The Jacobian for a symmetric perturbation is always positive. Figure 19 shows the variation of J_0 for anti-symmetric perturbations versus the fin heights h_L/a or h_W/a for $\theta_0 = 100°$ and $K = 5.5591$. The line with circles in figure 19 shows J_0 versus the leeward fin size h_L/a when a windward fin is not used ($h_W/a = 0$). Although a leeward fin with $h_L/a > 2.5$ greatly improves the stability of the vortices, a leeward fin alone cannot suppress vortex asymmetry whatever its size. The line with triangles shows J_0 versus h_W/a when the leeward fin is fixed with $h_L/a = 2.0$. Adding a windward fin

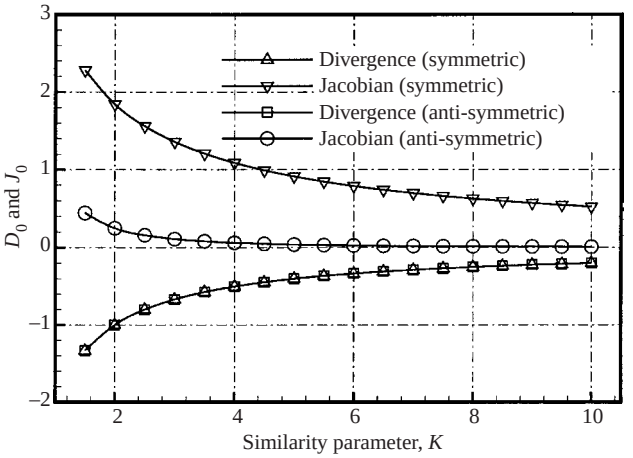

FIGURE 20. Divergence and Jacobian vs. similarity parameter for a flat-plate delta wing.

does not improve the stability of the vortices in this case. With a larger leeward fin $h_L/a = 3.0$, as shown by the line with squares in figure 19, however, the addition of a windward fin of the size $h_W/a \geqslant 2.2022$ makes the initial unstable vortices stable. Further calculations indicate that if $h_L/a \geqslant 2.6295$, there exists a windward fin of finite height that suppresses the vortex asymmetry, otherwise no such windward fin exists. Similarly, if $h_W/a \geqslant 2.1852$, there exists a leeward fin of finite height that suppresses the vortex asymmetry, otherwise no such leeward fin exists. If an equal height is required for the leeward and windward fin to suppress the vortex asymmetry, $h_L/a = h_W/a \geqslant 2.7259$.

4.3. *Slender flat-plate delta wing*

The stability of the stationary vortex pair over a slender flat-plate delta wing was studied by Huang & Chow (1996) using the same simplified vortex model but a different method of stability analysis. They gave the stationary symmetric vortex position and strength versus K and showed that the vortex flow is stable to small perturbations in the region $0.2 \leqslant K \leqslant 2.0$. The present stability theory is a convenient way to study this problem. The stationary vortex position and strength calculated by the present theory (Cai, Liu & Luo 2001*b*) exactly overlap with the solutions by Huang & Chow (1996) in the range of K calculated by them. However, an extended range of K from 0 to 10 is investigated in the present study.

Figure 20 shows that the symmetric vortex pair is stable to small symmetric and anti-symmetric perturbations for the entire range $0 < K \leqslant 10$. The degree of stability decreases monotonically as K increases and neutral stability is approached as K becomes large. Stahl (1993) carried out flow-visualization experiments in a water tunnel. The Reynolds number based on the length of the model is $Re_L = 2.8 \times 10^4$. The delta wing model has sharp edges, a semi-apex angle $\varepsilon = 8^\circ$, and angle of attack $\alpha = 38^\circ$ (i.e. $K = 5.5591$). The experiments show that the leading-edge separation vortices over the wing remain symmetric before vortex breakdown occurs on the wing. This agrees with the predictions of figure 20.

Smith & Clark (1975) showed that the two-dimensional inviscid incompressible flow around a flat plate normal to the free-stream velocity has no stationary symmetric vortices behind the plate. In the corresponding three-dimensional case, however, such stationary symmetric vortices do exist over the slender flat-plate delta wing. The

mechanism for the existence of such vortices in the three-dimensional case is the velocity $\boldsymbol{U}_c$ in (3.4) induced by the axial component of the free-stream velocity at the vortex, which tends to pull the vortex pair towards the centreline of the flat-plate delta wing.

Under anti-symmetric perturbations, the symmetric vortex pair is unstable for the slender circular cone and is stable for the slender flat-plate wing. The reason for this difference is due to the thickness effect of the circular cone in both the $\boldsymbol{U}_1$ and $\boldsymbol{U}_2$ parts of the solution discussed in § 3. The instability effect due to thickness of the circular cone in the normal flow part is similar to that for the circular cylinder in the free-stream flow, which is to push the vortices away from the body. In addition, the thickness of the circular cone also causes an effective expansion of the flow by a source term given in (3.7). In the light of this, flow suction at the surface of the circular cone might be used to help stabilize the symmetric vortex pair at high angles of attack.

4.4. *Slender flat-plate delta wing with fin*

Shanks (1963) in his subsonic flow measurements found that the leading-edge symmetric vortices over the flat-plate delta wing with $\varepsilon = 6^\circ$ and a centreline spline of height $h/s = 0.5$ became asymmetric at $\alpha \geqslant 24^\circ$. This contradicts the observations by Stahl *et al.* (1992). Ericsson (1992) claimed that the vortex asymmetry was not due to hydrodynamic instability but rather probably due to asymmetric reattachment in the presence of the centreline spline on the leeward side of Shanks' wing model. This controversy leads to the following study of vortex stability over the delta wing with a triangular flat-plate fin on the leeward side of the wing.

The contour of the slender flat-plate delta wing with a fin of height h in the cross-flow plane is mapped conformally into a circle by the following consecutive transformations:

$$Z = \frac{1}{2}\left(\rho - \frac{s^2}{\rho}\right), \tag{4.4}$$

$$\frac{1}{2}\left(\rho + \frac{s^2}{\rho}\right) - \xi_m = \frac{1}{2}\left(\zeta + \frac{\sigma^2}{\zeta}\right), \tag{4.5}$$

where

$$\xi_m = \frac{(s-h_s)^2}{4h_s}, \quad \sigma = \frac{(s+h_s)^2}{4h_s}, \quad h_s = h + (h^2+s^2)^{1/2}.$$

Here, the free-stream flow velocity U_n in the plane Z is transformed into $U_n/2$ in the plane ζ. The complex velocity at the vortex Z_1 in the plane Z is given by (4.3) with U_n replaced by $U_n/2$ and a replaced by s. The last term in (4.3) must be removed.

The divergence D_0 and the Jacobian J_0 at the stationary vortex position Z_0 under symmetric and anti-symmetric perturbations are evaluated from the complex velocity expression, and shown in figure 21 as a function of the fin height h/s for $K = 4.0$. It is seen that D_0 and J_0 are constants under symmetric perturbations as they should be. Under anti-symmetric perturbations, J_0 begins with a positive value but decreases to zero as h/s increases to 0.2216. It then becomes negative and remains negative until $h/s = 1.2474$. Thus, according to our stability theory, adding a small leeward side fin in the range $0.2216 < h/s < 1.2474$ causes the initially stable vortices over the delta wing to become unstable. Only when $h/s > 1.3059$ will the fin start to enhance the stability of the vortices compared to without the fin.

The front part of Shanks' wing model, from the apex as far back as $x = c_0/2$ (c_0 is the root chord of the wing), resembles a flat-plate delta wing with a flat-plate

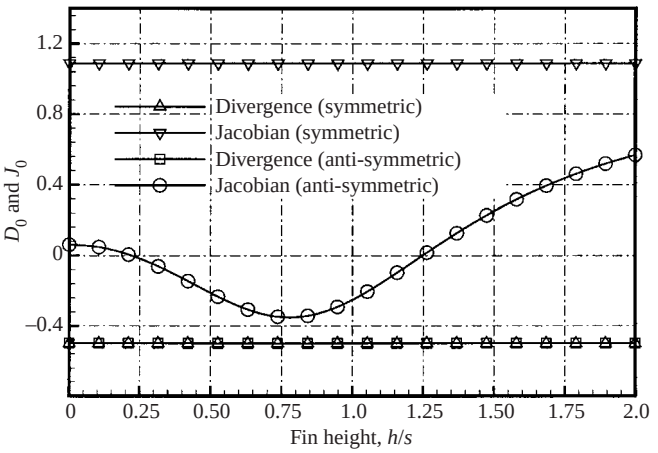

FIGURE 21. Divergence and Jacobian vs. fin height for a flat-plate delta wing with fin, $K = 4.0$.

triangular fin of height $h/s \approx 0.5$. In the rear part of the model, $1/2 \leqslant x/c_0 \leqslant 1$, the centreline spline has a constant height equal to that at $x = c_0/2$. In order to compare with Shank's experimental setup, two cases are studied by the present method: (i) $h/s = 0.2$ and (ii) $h/s = 0.5$. When $h/s = 0.2$, the onset of the vortex flow asymmetry is at $K = 4.4414$, and when $h/s = 0.5$, the onset is at $K = 2.4929$. The experimental onset for Shanks' model is at $K = 4.2361$. These results strongly suggest that the vortex asymmetry over Shanks' delta wing and most probably other slender conical bodies is due to hydrodynamic instability.

4.5. *Slender elliptic cone*

The flat-plate delta wing and the circular cone can be seen as limiting cases of an elliptic cone of thickness ratio τ (half-thickness/semi-span) as τ approaches 0 and 1, respectively. It is interesting to investigate how the stability property of the symmetric vortex flow over the slender elliptic cone changes from unstable to stable as the thickness ratio decreases from 1 to 0.

By using the conformal mapping relations already derived in § 2.4, the complex velocity of the vortex at Z_1 for the three-dimensional elliptic cone can be obtained as

$$u - \mathrm{i}v = \left[\frac{U_n}{2}(1 - 1/\zeta_1^2) + \frac{\mathrm{i}\Gamma}{2\pi}\left(-\frac{1}{\zeta_1 - \zeta_2} - \frac{1}{\zeta_1 - 1/\overline{\zeta_1}} + \frac{1}{\zeta_1 - 1/\overline{\zeta_2}}\right)\right]\left(\frac{\mathrm{d}\zeta}{\mathrm{d}Z}\right)_1 - \frac{\mathrm{i}\Gamma}{4\pi}\left(\frac{\mathrm{d}^2 Z}{\mathrm{d}\zeta^2}\right)_1\left(\frac{\mathrm{d}\zeta}{\mathrm{d}Z}\right)_1^2 - \frac{U_n\overline{Z_1}}{bK} + \frac{1}{2\pi}\sum_{j=1}^{n}\frac{Q_j}{Z_1 - Z_j}. \quad (4.6)$$

Stahl (1993) presented top and side views of the vortex configurations on the leeward side of the delta wing and the elliptic cones with the thickness ratio $\tau = 0.40$, 0.65 and 1.0, for $\varepsilon = 8^\circ$ at an angle of attack $\alpha = 38^\circ$ (i.e. $K = 5.5591$). The main results showed that the degree of asymmetry of the vortex flow behind the elliptic cones decreases as the cone becomes flatter.

To compare with the experimental observations, figure 22 plots D_0 and J_0 versus τ for the slender elliptic cone for $K = 5.5591$ and $\theta_0 = 90^\circ$. The vortices change from being unstable to stable as τ decreases from 1 to 0. The critical thickness ratio for this transition is $\tau = 0.389$. The agreement with Stahl's experimental observations is good considering the uncertainty in the separation position θ_0 in the experiments.

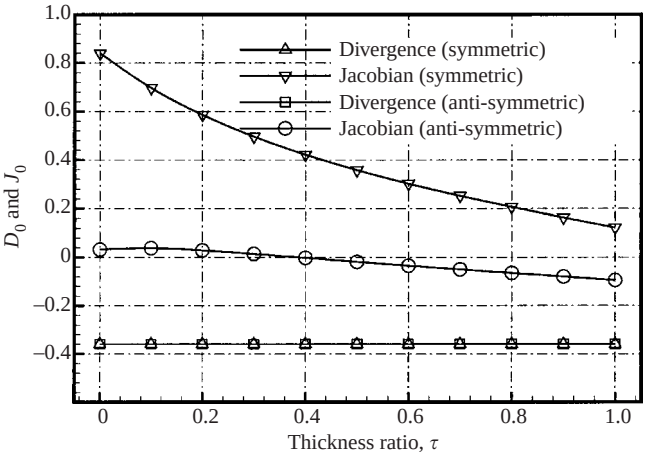

FIGURE 22. Divergence and Jacobian vs. thickness ratio for an elliptic cone, $K = 5.5591$, $\theta_0 = 90°$.

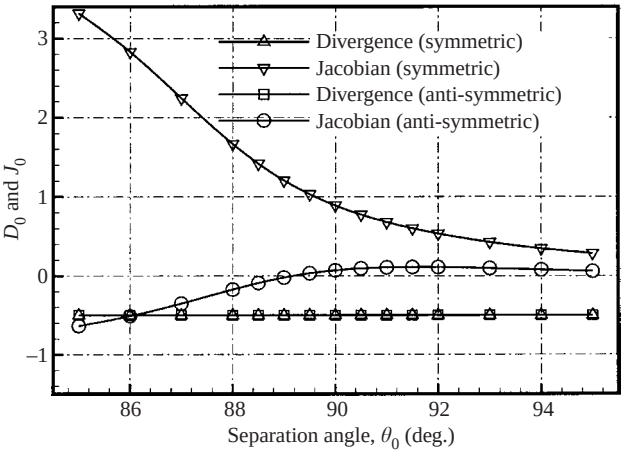

FIGURE 23. Divergence and Jacobian vs. separation angle for an elliptic cone, $\tau = 0.10$, $K = 4.0$.

Using tuft-grid surveys at low speeds, Bird (1969) observed that the asymmetric vortex flow over a slender flat-plate delta wing model with a rounded leading edge and a semi-apex angle $\varepsilon = 3.5°$ occurs at $\alpha \geqslant 15°$, which disagrees with the observations by Stahl *et al.* (1992), who used wing models with sharp leading edges. To investigate this controversy, a slender elliptic cone of thickness ratio $\tau = 0.1$ is considered for $K = 4.0$. The separation point may vary slightly around the round leading edge of the elliptic cone wing. Figure 23 plots the divergence D_0 and Jacobian J_0 vs. the separation angle θ_0. The vortices are stable when the separation is exactly at the leading edge of the wing ($\theta_0 = 90°$). When the separation point moves from the leading edge to the windward side ($\theta_0 > 90°$) the symmetric vortex pair remains stable, but when the separation point moves to the leeward side of the leading edge ($\theta_0 < 90°$), the vortices become less stable. They become neutrally stable at $\theta_0 = 89.17°$ and unstable when $\theta_0 < 89.17°$. The coordinates of this critical separation point ($\theta_0 = 89.17°$) are $x/b = 0.014337$ and $y/b = 0.989668$. They are very close to the coordinates

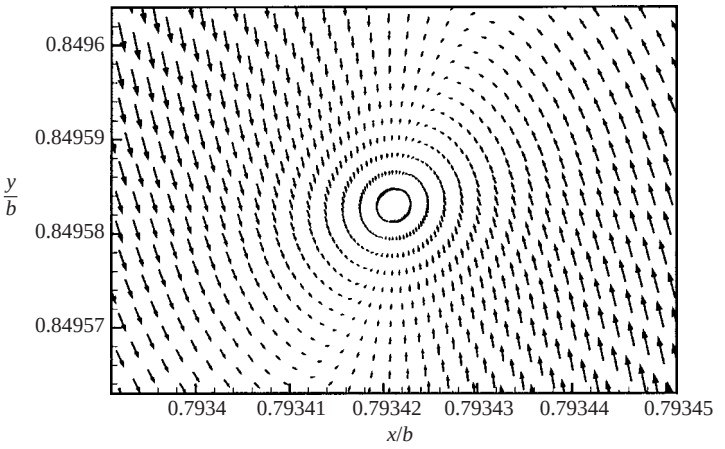

FIGURE 24. Velocity of a vortex under anti-symmetric perturbations for the flow over an elliptic cone, $\tau = 0.1$, $K = 4.0$, $\theta_0 = 90^\circ$ (stable case).

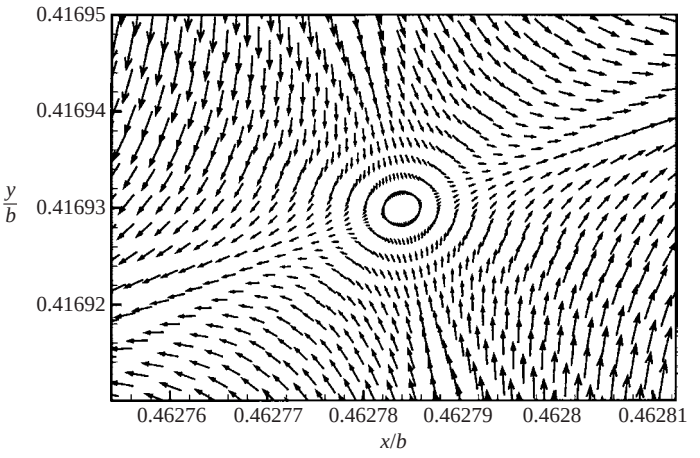

FIGURE 25. As figure 24 but for $\theta_0 = 85^\circ$ (unstable case).

of the leading edge, $x/b = 0$ and $y/b = 1.0$. Bird (1969) did not provide details of his wing profile nor measurements of separation angles. If his wing model were to be represented by our elliptic cone with $\tau = 0.1$, the critical separation angle would be $\theta_0 = 89.3^\circ$ for the experimental values $\varepsilon = 3.5^\circ$ and $\alpha = 15^\circ$ ($K = 4.38$). The asymmetry observed by Bird (1969) may be due to such slight changes in the separation position on the round leading edge of his experimental models. This agrees with the experimental results of Lim *et al.* (2001) on a flat-plate wing of ogive-shaped planform with sharp/rounded tip and edges. For lack of experimental data on the separation position, no further quantitative comparison of the present analyses with Bird's experimental results is made here. It is clear from the computations, however, that the symmetry configuration of the leading-edge separated vortex flow over a highly swept delta wing can be controlled by slightly changing the separation position around the leading edge.

To appreciate the physical meaning of the stability conditions in terms of D_0 and J_0, figures 24 and 25 show the vortex velocity field given by (4.6) under anti-symmetric

perturbations for the separation positions $\theta_0 = 90°$ and 85°, respectively. Compared to the two-dimensional cases shown in figures 7 and 8, the velocity vectors in figure 24 are drawn into the stationary point while circling around it. This is because the divergence D_0 is negative at the stationary point. Because of the positive J_0, the eigenvalue for the motion of the vortex contains an imaginary part that gives rise to the oscillatory motion.

Figure 25 shows an unstable case when $J_0 < 0$. Although D_0 is still negative in this case, a negative J_0 causes at least some velocity vectors to leave the stationary point, which leads to possible runaway of the vortex when slightly perturbed from its stationary location, similar to the situation shown in figure 7.

5. Conclusions

A general stability condition for vortices in an arbitrary two-dimensional flow is developed. This condition reproduces results on the stability of a pair of vortices behind a circular cylinder initially given by Föppl (1913) and later corrected by Smith (1973). This condition can be easily applied analytically or numerically to complex flow problems. It is applied to the problem of symmetric vortices behind circular cylinders with or without rear splitter plates and also to elliptic cylinders. A conical slender-body theory is then developed to reduce the study of stability of symmetric vortices over slender conical bodies at high angles of attack to a two-dimensional problem where the general stability condition may be applied. Slender circular cones and highly swept delta wings with and without fins, and slender elliptic cones of various eccentricities are studied. The following conclusions are drawn.

(*a*) The stability of any vortex or a vortex system for any given mode of small motion in a two-dimensional space can be determined by calculating the Jacobian and divergence of the vortex velocity field in terms of the location of the vortex under consideration. The stability conditions are listed in table 1.

(*b*) In an inviscid model with two concentrated symmetric vortices behind a circular or elliptic cylinder, no stationary points exist for which the separation angle is equal to or greater than 90° measured from the rear stagnation point of the cylinder. For three-dimensional circular or elliptic cones, however, stationary points exist for separation angles larger than 90°.

(*c*) A pair of stationary symmetric vortices behind a circular or elliptic cylinder is neutrally stable to symmetric perturbations, and is unstable to anti-symmetric perturbations. Adding a splitter plate of sufficient length behind a circular cylinder makes the vortices neutrally stable to anti-symmetric perturbations. However, a splitter plate of a short length below a critical length has destabilizing effects.

(*d*) It is proven that a pair of stationary symmetric vortices behind any two-dimensional profile is unstable or at best neutrally stable because the divergence of the vortex velocity field at the symmetric stationary points is always zero.

(*e*) Stationary symmetric vortices over circular cones are unstable to small anti-symmetric perturbations. This instability can be suppressed by adding a flat-plate triangular fin of sufficient height in the incidence plane of the cone. When the separation lines are located on the leeward side of the cone, a fin on the leeward side is sufficient. When the separation lines are on the windward side of the cone, fins on both leeward and windward sides are needed to suppress the vortex asymmetry. However, a fin of very low height added to a slender circular cone or a flat-plate delta wing destabilizes the vortex flow.

(*f*) For a highly swept sharp-edged flat-plate delta wing, the vortex flow over the wing is stable to small perturbations and thus remains symmetric before vortex breakdown occurs on the wing. However, with round leading edges, vortices are sensitive to slight changes of the separation position around the leading edge. A slight shift from the leading edge to a nearby point on the leeward side of the wing may lead to the onset of vortex asymmetry at some high angle of attack.

(*g*) For slender elliptic cones of various thickness ratios, the degree of vortex asymmetry decreases monotonically as the thickness ratio decreases from 1 to 0. There is a critical thickness ratio for a given similarity parameter and separation angle.

The authors are greatly indebted to the reviewers and the associate editor, Professor Sanjiva Lele, for their valuable comments and suggestions which significantly improved the quality of this paper.

Appendix. Proof of $D_0 = 0$ for any pair of symmetric vortices in two dimensions

The complex velocity of a general Föppl problem with a circular cylinder of radius a and two vortices, Γ_1 at ζ_1 and Γ_2 at ζ_2, can be written as

$$u - \mathrm{i}v = U\left(1 - \frac{a^2}{\zeta^2}\right) - \frac{\mathrm{i}\Gamma_1}{2\pi}\left[\frac{1}{\zeta - \zeta_1} - \frac{1}{\zeta - a^2/\overline{\zeta_1}}\right] - \frac{\mathrm{i}\Gamma_2}{2\pi}\left[\frac{1}{\zeta - \zeta_2} - \frac{1}{\zeta - a^2/\overline{\zeta_2}}\right]. \tag{A 1}$$

For vortices of strengths $-\Gamma$ and Γ, the vortex velocity for the vortex at ζ_1 is then

$$u - \mathrm{i}v = U\left(1 - \frac{a^2}{\zeta_1^2}\right) + \frac{\mathrm{i}\Gamma}{2\pi}\left[\frac{1}{\zeta_1 - a^2/\overline{\zeta_2}} - \frac{1}{\zeta_1 - \zeta_2} - \frac{1}{\zeta_1 - a^2/\overline{\zeta_1}}\right]. \tag{A 2}$$

Equations (A 1) and (A 2) reduce to (2.1) and (2.2), respectively, for a pair of symmetric vortices and a unit circle in the original Föppl problem.

Let ζ_0 and $\overline{\zeta_0}$ be points on the Föppl lines (symmetric stationary points). The vortex velocity for symmetric perturbations of the vortices is obtained by substituting $\zeta_1 = \zeta_0 + \Delta\zeta = \zeta$ and $\zeta_2 = \overline{\zeta_0} + \overline{\Delta\zeta} = \overline{\zeta}$ into (A 2),

$$u - \mathrm{i}v = F(\zeta, \overline{\zeta}) = U\left(1 - \frac{a^2}{\zeta^2}\right) + \frac{\mathrm{i}\Gamma}{2\pi}\left[\frac{1}{\zeta - a^2/\zeta} - \frac{1}{\zeta - \overline{\zeta}} - \frac{1}{\zeta - a^2/\overline{\zeta}}\right]. \tag{A 3}$$

The vortex velocity for anti-symmetric perturbations of the vortices is obtained by substituting $\zeta_1 = \zeta_0 + \Delta\zeta = \zeta$ and $\zeta_2 = \overline{\zeta_0} - \overline{\Delta\zeta} = 2\overline{\zeta_0} - \overline{\zeta}$ into (A 2),

$$u - \mathrm{i}v = F(\zeta, \overline{\zeta}) = U\left(1 - \frac{a^2}{\zeta^2}\right) + \frac{\mathrm{i}\Gamma}{2\pi}\left[\frac{1}{\zeta - a^2/(2\zeta_0 - \zeta)} - \frac{1}{\zeta - 2\overline{\zeta_0} + \overline{\zeta}} - \frac{1}{\zeta - a^2/\overline{\zeta}}\right]. \tag{A 4}$$

Although $F(\zeta, \overline{\zeta})$ is not analytic with respect to ζ as a whole, $F(\zeta, \overline{\zeta})$ can be regarded as partial functions of ζ and $\overline{\zeta}$ and it is easily shown by direct differentiation and the chain rule that

$$\left(\frac{\partial u}{\partial \xi} + \frac{\partial v}{\partial \eta}\right) + \mathrm{i}\left(\frac{\partial u}{\partial \eta} - \frac{\partial v}{\partial \xi}\right) = 2\frac{\partial F}{\partial \overline{\zeta}}.$$

It is easily verified that the real part of $\partial F/\partial\overline{\zeta}$ is zero at any symmetric stationary point for both the symmetric and anti-symmetric perturbation cases given in (A 3) and (A 4), proving that D_0 is zero for the Föppl problem.

The flow field past any two-dimensional profile can be obtained from that of the Föppl problem via a conformal mapping from ζ to Z. Stationary points are preserved under such a conformal mapping. The vortex velocity field in the $Z = x + \mathrm{i}y$ plane is then given by (2.7), which can be written in terms of $F(\zeta, \overline{\zeta})$ for the Föppl problem as

$$u - \mathrm{i}v = F(\zeta, \overline{\zeta})\frac{\mathrm{d}\zeta}{\mathrm{d}Z} - \frac{\mathrm{i}\Gamma}{4\pi}\frac{\mathrm{d}^2 Z}{\mathrm{d}\zeta^2}\left(\frac{\mathrm{d}\zeta}{\mathrm{d}Z}\right)^2. \tag{A 5}$$

Notice that if $\zeta = f(Z)$ is analytic, then $\mathrm{d}\overline{\zeta}/\mathrm{d}\overline{Z}$ exists and in addition, $\mathrm{d}\overline{\zeta}/\mathrm{d}\overline{Z} = \overline{(\mathrm{d}\zeta/\mathrm{d}Z)}$. Again by direct differentiation and the chain rule, we obtain

$$\left(\frac{\partial u}{\partial x} + \frac{\partial v}{\partial y}\right) + \mathrm{i}\left(\frac{\partial u}{\partial y} - \frac{\partial v}{\partial x}\right) = 2\overline{\left(\frac{\mathrm{d}\zeta}{\mathrm{d}Z}\right)}\left(\frac{\mathrm{d}\zeta}{\mathrm{d}Z}\right)\left(\frac{\partial F}{\partial \overline{\zeta}}\right) = 2\left|\frac{\mathrm{d}\zeta}{\mathrm{d}Z}\right|^2\left(\frac{\partial F}{\partial \overline{\zeta}}\right).$$

Since the real part of $\partial F/\partial\overline{\zeta}$ is zero at any symmetric stationary point for both symmetric and anti-symmetric perturbations in the Föppl problem, the above equation proves that D is zero for a pair of vortices at their symmetric stationary points in the flow past any two-dimensional profile.

REFERENCES

Adams, M. C. 1953 Leading-edge separation from delta wing at supersonic speeds. *J. Aero. Sci.* **20**, 430–431.

Asghar, A., Stahl, W. H. & Mahmood, M. 1994 Suppression of vortex asymmetry and side force on a circular cone. *AIAA J.* **32**, 2117–2120.

Bernhardt, J. E. & Williams, D. R. 1998 Proportional control of asymmetric forebody vortices. *AIAA J.* **36**, 2087–2093.

Bird, J. D. 1969 Tuft-grid surveys at low speeds for delta wing. *NASA TN* D-5045.

Bradshaw, P. 1970 *Experimental Fluid Mechanics*, plate 5, p. 149. Pergamon Press.

Cai, J., Liu, F. & Luo, S. 2001*a* Stability of symmetric vortices behind two-dimensional bodies. *AIAA Paper* 2001–2844.

Cai, J., Liu, F. & Luo, S. 2001*b* Stability of symmetric vortices over slender conical bodies at high angles of attack. *AIAA Paper* 2001–2845.

Degani, D. 1992 Instabilities of flows over bodies at large incidence. *AIAA J.* **30**, 94–100.

Degani, D. & Levy, Y. 1992 Asymmetric turbulent vortical flows over slender bodies. *AIAA J.* **30**, 2267–2273.

Degani, D. & Tobak, M. 1992 Experimental study of controlled tip disturbance effect on flow asymmetry. *Phys. Fluids* A **4**, 2825–2832.

Dyer, D. E., Fiddes, S. P. & Smith, J. H. B. 1982 Asymmetric vortex formation from cones at incidence – a simple inviscid model. *Aero. Q.* **31**, 293–312.

Edwards, O. R. 1978 Northrop F-5F shark nose development. *NASA CR*-158936.

Ericsson, L. E. 1992 Sources of high alpha vortex asymmetry at zero sideslip. *J. Aircraft* **29**, 1086–1090.

Ericsson, L. E. & Reding, J. P. 1992 Asymmetric flow separation and vortex shedding on bodies of revolution. *Tactical Missile Aerodynamics: General Topics*, 2nd edn. (ed. M. J. Hemsch). *Prog. Astro. Aero.* **141**, 391–452.

Fiddes, S. P. 1980 A theory of the separated flow past a slender elliptic cone at incidence. *Computation of Viscous–Inviscid Interactions, Paper 30, AGARD CP*291.

Fiddes, S. P. & Williams, A. L. 1989 Recent developments in the study of separated flow past slender bodies at incidence. In *Symp. on the Prediction and Exploitation of Separated Flow*, pp. 31.1–31.17. Royal Aeronautical Society.

Föppl, L. 1913 Wirbelbewegung hinter einem kreiszylinder. *Sitzb. d. k. baeyr, Akad. d. Wiss., Math-Physi. Klasse, Müchen* **1**, 1–17.

Goldstein, S. 1938 *Modern Developments in Fluid Dynamics*, Vol. II, pp. 552–553. Oxford University Press.

Huang, M. K. & Chow, C. Y. 1996 Stability of leading-edge vortex pair on a slender delta wing. *AIAA J.* **34**, 1182–1187.

Keener, E. R. & Chapman, G. T. 1977 Similarity in vortex asymmetries over slender bodies and wings. *AIAA J.* **15**, 1370–1372.

Lamb, H. 1932 *Hydrodynamics*, 6th edn., p. 223. Cambridge University Press.

Legendre, R. 1953 Écoulement au voisinage de la pointe aavant d'une aile a forte fléche aux incidences moyennes. *La Recherche Aeronautique, Bulletin Bimestriel, De L'Office National D'Études Et De Recherches Aeronautiques*, Jan.–Feb.

Levy, Y., Hesselink, L. & Degani, D. 1996 Systematic study of the correlation between geometrical disturbances and flow asymmetries. *AIAA J.* **34**, 772–777.

Lim, T. T., Lua, K. B. & Luo, S. C. 2001 Role of tip and edge geometry on vortex asymmetry. *AIAA J.* **39**, 539–543.

Lowson, M. V. & Ponton, A. J. C. 1992 Symmetry breaking in vortex flows on conical bodies. *AIAA J.* **30**, 1576–1583.

Milne-Thomson, L. M. 1968 *Theoretical Hydrodynamics*, 5th edn., p. 370. Macmillan.

Ng, T. T. 1990 Effect of a single strake on the fore body vortex asymmetry. *J. Aircraft* **27**, 844–846.

Pidd, M. & Smith, J. H. B. 1991 Asymmetric vortex flow over circular cones. In *Vortex Flow Aerodynamics, AGARD CP*-494, July 1991, pp. 18-1–18-11.

Polhamus, E. C. 1971 Predictions of vortex-lift characteristics by a leading-edge suction analogy. *J. Aircraft* **8**, 193–199.

Roshko, A. 1961 Experiments on the flow past a circular cylinder at very high Reynolds number. *J. Fluid Mech.* **10**, 345–356.

Rossow, V. L. 1978 Lift enhancement by an externally trapped vortex. *J. Aircraft* **15**, 618–625.

Saffman, P. G. 1992 *Vortex Dynamics*, pp. 22, 43. Cambridge University Press.

Shanks, R. E. 1963 Low-subsonic measurements of static and dynamic stability derivatives of six flat-plate wing having leading-edge sweep angles of 70° to 84°. *NASA TN* D-1822.

Smith, A. C. 1973 On the stability of Föppl's vortices. *J. Appl. Mech.* **40**, 610–612.

Smith, J. H. B. & Clark, R. W. 1975 Non-existence of stationary vortices behind a two-dimensional normal plate. *AIAA J.* **13**, 1114–1115.

Stahl, W. H. 1990 Suppression of vortex asymmetry behind circular cones. *AIAA J.* **28**, 1138–1140.

Stahl, W. H. 1993 Experimental investigations of asymmetric vortex flows behind elliptic cones at incidence. *AIAA J.* **31**, 966–968.

Stahl, W. H., Mahmood, M. & Asghar, A. 1992 Experimental investigations of the vortex flow on delta wings at high incidence. *AIAA J.* **30**, 1027–1032.

Sychev, V. V. 1960 Three-dimensional hypersonic gas flow past slender bodies at high angle of attack. *J. Maths Mech. (USSR)* **24**, 296–306.

Tang, S. & Aubry, N. 1997 On the symmetry breaking instability leading to vortex shedding. *Phys. Fluids* **9**, 2550–2561.

Thomson, K. D. & Morrison, D. F. 1971 The spacing, position and strength of vortices in the wake of slender cylindrical bodies at large incidence. *J. Fluid Mech.* **50**, 751–783.

Van Dyke, M. 1982 *An Album of Fluid Motion*. Parabolic Press.

Zilliac, G. G., Degani, D. & Tobak, M. 1991 Asymmetric vortices on a slender body of revolution. *AIAA J.* **29**, 667–675.